Efficient design and implementation of a distributed temperature sensor for field apparatus

OPEN ACCESS
IOP Publishing
Measurement Science and Technology
Meas. Sci. Technol. **33** (2022) 095204 (9pp)
https://doi.org/10.1088/1361-6501/ac79a6

Efficient design and implementation of a distributed temperature sensor for field apparatus

Qigong He[1,*], Yuanjie Yue[2] and Xiaodong Jia[3]

[1] School of Electronics and Information Engineering, Beihang University, Beijing 100191, People's Republic of China
[2] Tianjin Technician Institute of Mechanical and Electrical Technology, Tianjin 300201, People's Republic of China
[3] Tianjin Jinhang Institute of Technical Physics, Tianjin 300300, People's Republic of China

E-mail: havana.hq@163.com

Received 13 December 2021, revised 12 June 2022
Accepted for publication 16 June 2022
Published 29 June 2022

Abstract

The signal acquisition and processing ability of distributed temperature sensor based on Raman scattering (DTS-Raman) directly determines the accuracy, spatial resolution, temperature resolution, and other key indicators of the entire system. Real-time and effective processing is the key to ensuring the practicability of the field system. Owing to the long distance of the DTS system, the energy of the weak Raman scattering is further reduced when it reaches the avalanche photodiode detector because of fiber loss, which results in a decrease in the signal-to-noise ratio (SNR) and an increase in the temperature measurement error. To improve the SNR and ensure the accuracy of the demodulation temperature, the signal acquisition and processing module must be able to perform real-time and fast processing of large amounts of data. The existing processing structure based on the acquisition board requires a special personal computer and host processing software, which limits the application of DTS system. Therefore, a real-time acquisition and processing scheme based on field-programmable gate array is proposed in this paper. A set of cyclic shift register sequence (CSRS) with Ping-Pang functions is designed to improve the storage efficiency. According to the period of the laser source, the accumulated results stored in the CSRS and echo pulse data are accumulated and shifted in real time to realize circular utilization of storage resources. A DTS-Raman system prototype and test platform are built to verify the effects of the proposed scheme. The experimental results show that the scheme can realize a temperature accuracy within $\pm 0.475\ ^{\circ}C$ in real time and has a high resource utilization efficiency.

Keywords: optical fiber sensor, Raman scattering, distributed temperature sensor (DTS), cyclic shift register sequence (CSRS), field programmable gate array (FPGA), real-time processing

(Some figures may appear in colour only in the online journal)

* Author to whom any correspondence should be addressed.

1. Introduction

Optical fiber sensing technology begins in 1977 and has rapidly developed with the development of optical fiber communication technology. It is a new sensing technology that uses optical signals as information carriers and optical fibers as transmission media to sense and transmit all types of measurement signals in an environment [1]. Compared with traditional point sensors, optical fiber sensing technology has the unique advantages of being distributed, highly stable, highly integrated, long-distance, anti-interference, waterproof and moisture-proof [2]. It can continuously measure various environmental parameters around a transmission medium and obtain distribution information that vary with the time and space. In recent years, it has been widely used by the industry and other fields, such as power cables, subway pipe corridors/power tunnels, dams, and other construction safety [3–9].

The distributed temperature sensor (DTS) system is an application of optical fiber sensing technology in the field of temperature measurement [10], and is first proposed by Southampton University in the UK in 1981 [11]. Optical fiber has the characteristics of small volume, light weight, good electrical insulation, flexible bending, corrosion resistance, large measurement range and high sensitivity [12]. Temperature measurement system based on optical fiber sensing technology has the characteristics of fast response, wide frequency band, explosion-proof, flame-proof, and anti-electromagnetic interference [13–15]. Therefore, the DTS system has attracted the attention of scientific and technological personnel in various countries and has conducted systematic and in-depth research [16–18]. McDaniel *et al* [19] presented and systematically analyzed a dynamic, double-ended calibration routine developed in response to site-specific challenges and constraints. Bazzo *et al* [20] presented a deconvolution algorithm based on a linear DTS model, and developed a total variation regularization to improve the spatial resolution of a DTS based on Raman scattering (DTS-Raman) system. Jian *et al* [21] proposed and experimentally demonstrated a DTS-Raman with a heat transfer functional model to perceive the surrounding temperature in advance, which solved the temperature hysteresis effect of a multi-mode fiber under different temperature conditions.

Although the DTS system has many advantages, owing to the weak light intensity of Raman scattering, the signal-to-noise ratio (SNR) of the echo signal reaching the avalanche photodiode (APD) detector is low, which seriously affects the accuracy of temperature demodulation. To improve the signal SNR, the echo pulse must be accumulated several times and then averaged. The computational burden of the signal acquisition and processing units will be increased, which requires higher real-time performance of the processing unit for transmission and computation. The above studies can achieved real-time measurements to a large extent with a certain measurement accuracy. However, the processing architecture based on an acquisition board requires a special personal computer (PC) and host processing software [22], which greatly affects its cost and application scenario.

For special safety application such as subway and electric power, DTS system should not only complete temperature monitoring quickly and accurately, but also has flexible control functions such as fiber breaking alarm and automatic fire fighting to form a closed-loop control system. Speed performance of new components and flexibility inherent of all programmable solutions provide an appropriate solution such as microprocessors, digital signal processor (DSP) and field programmable gate array (FPGA). Especially with the fast progress of very large scale integration technology in recent years, the integration density, reliability and thermal efficiency of FPGA are higher and higher, while the power consumption and cost are lower and lower. It makes FPGA can not only significantly improve the execution efficiency of the algorithm by designing a special parallel architecture, but also use its rich input/output pin (I/O) resources to complete flexible control functions, reduce the cost of the control system and improve the performance level. Therefore, FPGA technology is now considered by an increasing number of designers in various fields of application such as image and signal processing, medical equipment and aircraft embedded control systems.

Based on this background, an efficient signal acquisition and processing scheme based on FPGA technology is proposed in this paper, which enhances the real-time processing ability of DTS-Raman system and improves the resource utilization efficiency of FPGA. In the scheme, a real-time processing method based on the cyclic shift register sequence (CSRS) with the Ping-Pang function is designed. And in each laser emission cycle, the echo pulse data accumulated in CSRS is accessed circularly to realize the recycling of storage resources. The experimental results verify that the scheme has efficient real-time processing ability and universality.

2. Distributed temperature sensing principle based on light scattering

According to the theoretical analysis and mathematical derivation in [23], the intensity formulas of Stokes and anti-Stokes light in spontaneous Raman scattering are as follows:

$$i_{\mathrm{as}} = \frac{N_0}{\gamma_{\mathrm{as}}^4 (\mathrm{e}^{h\Delta\gamma/kT} - 1)} \tag{1}$$

$$i_{\mathrm{s}} = \frac{N_0}{\gamma_{\mathrm{s}}^4 (1 - \mathrm{e}^{-h\Delta\gamma/kT})} \tag{2}$$

where γ_{s} and γ_{as} are the Stokes and anti-Stokes light wave numbers, respectively, $\Delta\gamma$ is the Raman frequency shift, and is 1.32×10^{13} Hz in the quartz fiber, where h is the Planck constant, k is the Boltzmann constant, and T is the absolute temperature of the environment. N_0 is independent of the ambient temperature and is determined only by the incident light intensity and the structure and physical characteristics of the optical fiber itself. Furthermore, the ratio of the two optical signals is [23]:

$$R(T) = \left(\frac{\lambda_s}{\lambda_{as}}\right)^4 \cdot e^{-\frac{h\Delta\gamma}{kT}} \quad (3)$$

where λ_s and λ_{as} are Stokes and anti-Stokes wavelengths respectively.

It can be seen that the ratio of anti-Stokes to Stokes light intensity in Raman scattering is only a function of the ambient temperature where the fiber is located. Thus, the temperature distribution can be solved by extracting the Stokes and anti-Stokes light intensity ratios at each point in the optical fiber distribution field. Simultaneously, combined with the principle of pulse laser detection, the spatial positions of the temperature points can be easily obtained.

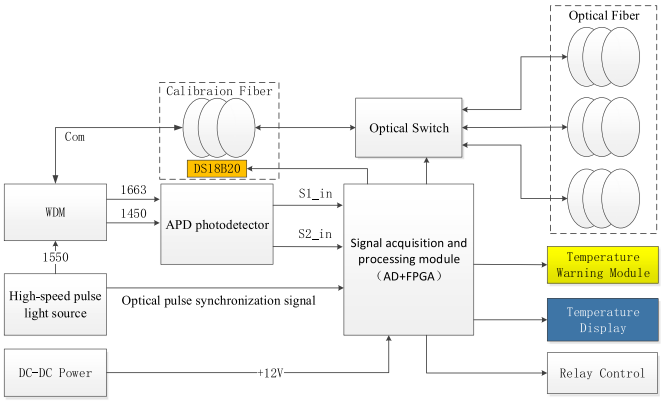

Figure 1. DTS-Raman model.

3. DTS-Raman system scheme based on CSRS

3.1. DTS-Raman system model

The DTS-Raman system is composed of a high-speed pulse light source, wavelength division multiplexer (WDM), calibration fiber, sensing fiber, APD photoelectric detection module, signal acquisition and processing module, optical switch, and reference temperature sensor, as shown in figure 1. Typically, multiple circuits are laid in a pipe gallery and tunnel simultaneously, and each circuit includes several optical cables. Therefore, it is necessary to expand the temperature measurement channel by using an optical switch. The calibration fiber is wound in the calibration box of the chassis, and the built-in temperature sensor collects the ambient temperature of the calibration fiber as the reference temperature to calibrate the measured temperature.

The DTS-Raman system works based on optical time domain reflectometer (OTDR) technology and belongs to the intensity modulation optical fiber sensing system. The optical signal intensity changes with ambient temperature along the optical fiber laying line. The working process is as follows: under the control of the signal acquisition and processing module, the high-speed pulse light source generates a series of narrow pulse lasers according to a certain repetition frequency cycle, obtains a 1550 nm pulse laser after modulation, and simultaneously feeds back the optical pulse synchronization signal to the control circuit at the same time. The 1550 nm pulsed laser is incident onto the optical fiber through the coupler in the WDM and transmitted along the entire optical fiber.

Scattering occurs during the transmission process in which the backscattered light opposite to the propagation direction of the incident light returns to the coupler of the WDM. After the stray light and interference light are filtered by the light splitter and filter, the anti-Stokes and Stokes light with Raman scattering center wavelengths of 1450 nm and 1663 nm in the combined optical signal are filtered to enter the dual-channel photoelectric detection module to convert the weak optical signal carrying temperature information into an electrical signal. It is then amplified by the amplification circuit, collected, and processed by the signal acquisition and processing module.

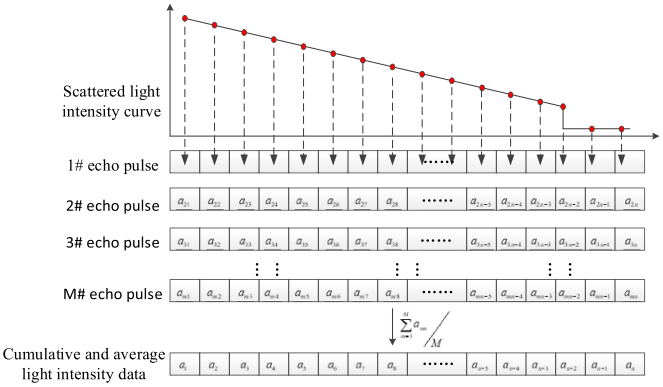

Figure 2. DTS-Raman system noise suppression processing scheme.

3.2. DTS-Raman system noise suppression scheme

After long-distance distributed optical fiber reflection, the returned Raman scattering signal is weak, resulting in a low SNR of the optical signal received by the APD detector. To ensure the demodulation performance, it is necessary to suppress the noise according to the characteristics of the signal and noise in the signal acquisition and processing modules to improve the overall SNR.

Generally, the cumulative average method is used to suppress noise, circularly accumulate multiple sampling results of backscattered light intensity in the same physical space, extract useful Raman signals after removing the noise, and reduce the impact of noise on resolution and sensitivity. The cumulative average process is shown in figure 2.

Triggered by the synchronization signal of the high-speed pulse light source, the information acquisition and processing module collects and stores the backscattered light signal from a fixed point on the optical fiber. The acquisition depth is determined using the optical fiber length and acquisition speed. Each time the light source emits an optical pulse, it begins to acquire and store it. After the number of optical signals collected and stored reaches the set cumulative times, it starts to accumulate and averages the stored scattered light pulse signals according to the corresponding

Table 1. Xilinx Zynq-7020 product table.

—	Source name	Parameter
Processing system (PS)	Processor core	Dual-core ARM, Cortex-A9 MPCore, up to 866 MHz
	L1 cache	32 KB instruction, 32 KB data per processor
	On-chip memory	256 KB
	Peripherals	2× UART, 2× SPI, 4× 32b GPIO
Programmable logic (PL)	Logic cells	85 K
	Look-up tables	53 200
	Flip-flops	106 400
	Total block RAM	4.9 Mb
	DSP slices	220

sampling time to obtain denoised backscattered light intensity data.

To ensure the resolution and accuracy, the accumulation times must be large, which puts forward high requirements for the data processing capacity and resource requirements of the system signal acquisition and processing module. To solve this problem, many scholars [24] have used high-speed data acquisition cards to collect the backscattered light and transmit them to the host computer in real time for further denoising and demodulation. This scheme needs to be equipped with a special PC and processing software, which makes the system more complex, is not conducive to miniaturization, and limits its application scenario.

To solve the problem, a DTS information processing circuit integrating signal acquisition and processing using the architecture of 'ADC + FPGA' is proposed. The scheme selects a new-generation product of Xilinx Zynq-7020 with low cost, high performance, and multi-core processing capability as the core processor to meet the high performance requirements in the design and application. In fact, other similar system on a chip (SoC) can also be used to realize this structure. As an example, table 1 shows the parameters of Xilinx Zynq-7020.

By constructing CSRS on the programmable logic side for pipeline design, the control and processing are integrated, and the collected data are accumulated and stored in real-time, which greatly improves the resource utilization efficiency of the hardware platform. An internal signal-processing block diagram of the FPGA is shown in figure 3.

To trigger the system, a synchronous pulse fed back by the pulse laser module is used as the trigger signal to periodically control the CSRS for cyclic reading and writing under the control of service control timing. To ensure synchronization between the CSRS reading and writing and real-time sampling data, the CSRS control logic must be specially designed and constrained to avoid cumulative dislocation caused by synchronization time dislocation.

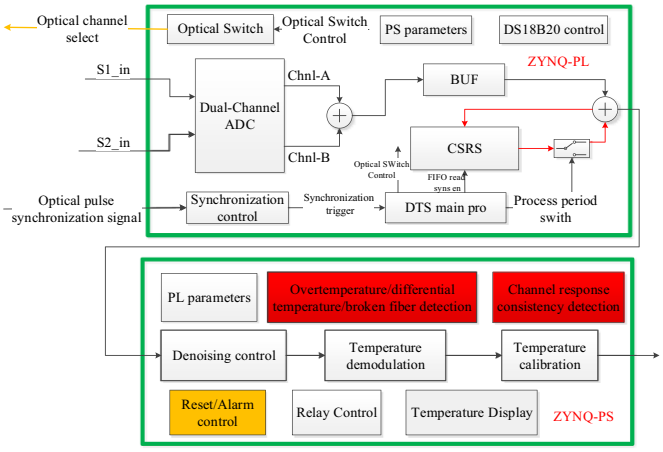

Figure 3. Signal processing block diagram of Zynq-7020.

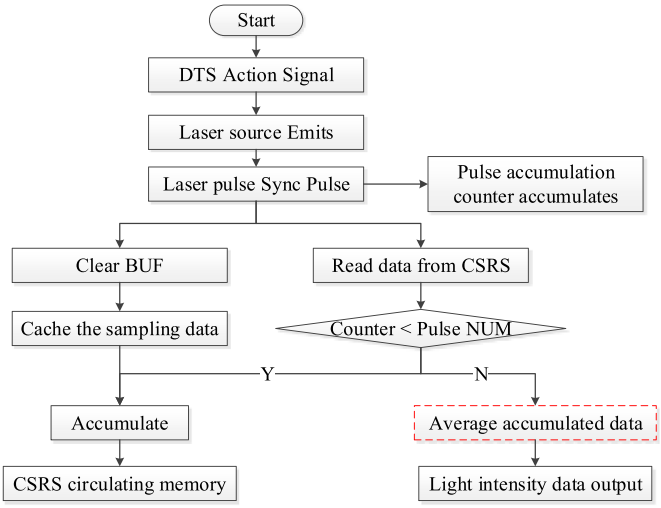

Figure 4. Flow chart of DTS cumulative average denoising control.

3.3. Denoising control flow based on CSRS

After the DTS-Raman system is powered on, the high-speed pulse light source emits a narrow pulse laser with a certain width and pulse interval under the control of the FPGA and simultaneously feeds back a synchronization signal to the FPGA. Then, FPGA uses the synchronization signal to count the accumulated pulses in real time and controls the CSRS to shift, read, and collect the stored optical pulse data. After accumulating the optical pulse data collected using high-speed analog-to-digital converter (ADC), it is pushed into the CSRS again. The control flow is illustrated in figure 4.

For the collected signal $s(n)$, the amplitude after M times of accumulation becomes $Ms(n)$. While the effective value is $\sqrt{M}s(n)$ for the random Gaussian white noise. Therefore,

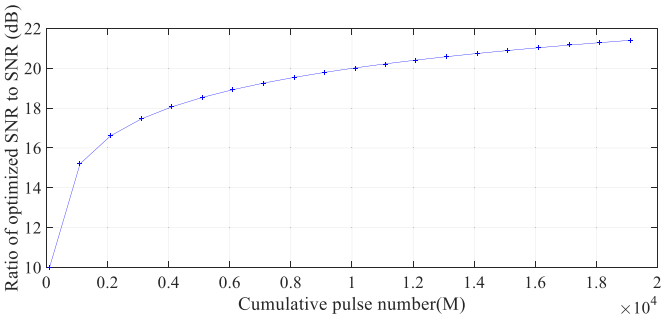

Figure 5. Optimized SNR improvement effect.

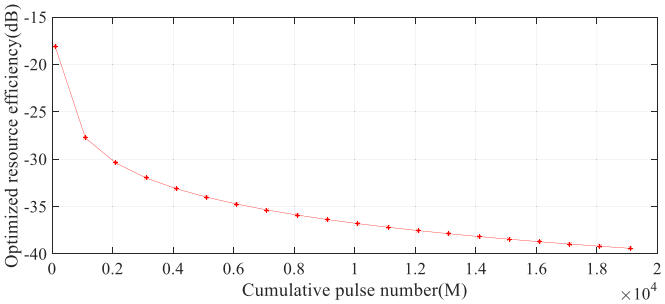

Figure 6. The variation curve of resource optimization efficiency with M.

according to the definition of SNR, after M times of cumulative average, the SNR is [25]:

$$\mathrm{SNR}' = \frac{Ms(n)}{\sqrt{M}s(n)} = \sqrt{M}\mathrm{SNR}. \tag{4}$$

On the other hand, the CSRS makes the $MN_\mathrm{L}N_\mathrm{B}$ storage resources required be $N_\mathrm{L}(N_\mathrm{B} + \log_2(M))$ for M times accumulation, where N_B is the ADC bit width, and N_L is the number of single sampling points. Figures 5 and 6 show the variation of optimized SNR improvement effect and resource optimization efficiency with M respectively.

It can be seen from the figure that the CSRS accumulation structure greatly improves the SNR and storage resource utilization efficiency of FPGA. So it can detect in a wider range under the same resources. Considering the cost and application requirements, the design detection distance in this paper is 10 km.

At the same time, in the CSRS structure, the accumulation process is carried out in the form of pipeline according to the luminous cycle of laser source. The single temperature measurement time mainly depends on the accumulated pulse number and laser repetition frequency, so the change of maximum fiber span will not lead to the increase of cumulative processing time of the algorithm. However, it is undeniable that in order to adapt to the increase of maximum fiber span, the repetition frequency of the laser must decrease, resulting in the increase of measurement time in the same cumulative pulse number. The variation relationship between running time and pulse repetition frequency (PRF), M and span is shown in table 2.

Table 2. The variation relationship between running time and PRF, M and max span.

Max span (km)	PRF (kHz)	M	Running time (s)
$\leqslant$10	10	1000	0.1
$\leqslant$10	10	10 000	1
10–20	5	1000	0.2
10–20	5	10 000	2

3.4. Temperature demodulation and calibration

In the scheme, an accumulated average algorithm is used to denoise the collected data, and Stokes light is used as a reference for temperature demodulation. The demodulated temperature is compensated for the different propagation losses of Stokes and anti-Stokes light in the optical fiber.

Theoretically, the ratio of the two Raman signals to the temperature is approximately a linear equation as:

$$T = H \times \frac{I_\mathrm{as}}{I_\mathrm{s}} + T_0 \tag{5}$$

where I_as and I_s are the strengths of anti-Stokes and Stokes signals, H and T_0 are the slope and intercept of the curve.

When temperature is same, the curve of demodulation temperature is horizontal. While, because the intensity of the anti-Stokes and Stokes signals received by APD are not the light intensity at the physical sampling point where scattering occurs in the optical fiber, there is a difference between the curve and theoretical curve. According to optical fiber transmission theory, when Raman scattering at the APD is detected by the receiving end, the intensities I_{ax} and I_{sx} are:

$$I_{ax} = I_\mathrm{as} \times 10^{-\frac{\alpha_\mathrm{as}}{10}x}\, I_{sx} = I_\mathrm{s} \times 10^{-\frac{\alpha_\mathrm{s}}{10}x} \tag{6}$$

where α_as and α_s are the attenuation coefficients corresponding to the anti-Stokes and Stokes light in the optical fiber, respectively. The intensity ratio of the two Raman scattering light signals at the APD receiver is:

$$\frac{I_{ax}}{I_{sx}} = \frac{I_\mathrm{as}}{I_\mathrm{s}} \times 10^{-\frac{\alpha_\mathrm{as}-\alpha_\mathrm{s}}{10}x}. \tag{7}$$

Furthermore, the loss compensation expression of demodulation temperature is:

$$T_x = H \times \frac{I_{ax}}{I_{sx}} \times 10^{\frac{\alpha_\mathrm{as}-\alpha_\mathrm{s}}{10}x} + T_0. \tag{8}$$

Therefore, the temperature information is demodulated by the ratio of the anti-Stokes signal to the Stokes signal, which is corrected to 10 at the bottom, and the positioning is realized by OTDR. The main steps are as follows:

(a) Extracting the temperature value of the reference temperature sensor.
(b) Extract the demodulation temperature within the distance of the calibration optical fiber and calculate the average demodulation temperature of each temperature measuring point of the calibration optical fiber.

(c) Loss compensation: compensate the loss of the original light intensity ratio curve according to equation (8), and the compensation relationship is:

$$T'_x = T_x \times 10^{\alpha_d \times x} \tag{9}$$

where α_d is the optical fiber loss attenuation compensation coefficient, x is the actual distance from the optical fiber temperature sampling point to the receiving end.

(d) Adjust the flatness of the original temperature curve:

$$T'_x = T_x \times \mathrm{e}^{a \times 10^{-bx^2} + (p-c) \times x + d} \tag{10}$$

where p is the flattening compensation coefficient of the light-intensity curve, which is related to the optical fiber, a, b, c, d are the fitting coefficients of the curve.

(e) Consistency compensation for the distance response of the original temperature curve: to solve the problem of inconsistent responses of different temperature measuring points to the same temperature, combined with the attenuation compensation scheme proposed in [16], consistency compensation is performed for the temperature curve, and the compensation relationship is:

$$T''_x = (A \times x + B) \times T'_x + C \times x + D \tag{11}$$

where A, B, C and D are the compensation coefficients to be calibrated.

(f) Temperature curve calibration: according to the actual environment of the optical fiber, compare and fit the final calculated temperature value with the actual calibration temperature, and calibrate the temperature value in the solution:

$$T'''_x = k \times T''_x + T_0 \tag{12}$$

where k and T_0 are the coefficients of the linear calibration curve, and T_0 includes the calibration difference between the temperature value of the reference temperature sensor and the average value of the calibrated optical fiber temperature.

In the actual implementation process, the light intensity for demodulation is the cumulative average light intensity:

$$\frac{I_{\mathrm{as}}}{I_{\mathrm{s}}} = \frac{\sum_{i=1}^{N} I_{\mathrm{as}i} \Big/ N}{\sum_{i=1}^{N} I_{\mathrm{s}i} \Big/ N} = \frac{\sum_{i=1}^{N} I_{\mathrm{as}i}}{\sum_{i=1}^{N} I_{\mathrm{s}i}}. \tag{13}$$

Therefore, the process of averaging the accumulated CSRS data can be offset, and the accumulated light intensity data can be directly used for temperature demodulation to further reduce the resources of the signal acquisition and processing module.

In addition to the above correction, spatial resolution is also one of the important indicators of DTS system, which determines the minimum distance interval that the system can perceive. Therefore, it should be taken into account in the system design. Generally, the spatial resolution of DTS system is determined by the laser pulse width τ_{w}, APD response bandwidth B, ADC sampling rate f_{s} and other factors, which can be simply expressed as [26]:

$$\delta R = \max\{\delta R_{\mathrm{p}}, \delta R_{\mathrm{B}}, \delta R_{\mathrm{s}}\} = \max\left\{\frac{\tau_{\mathrm{w}} c}{2n}, \frac{\tau_{\mathrm{r}} c}{2n}, \frac{\tau_{\mathrm{s}} c}{2n}\right\} \tag{14}$$

where, δR_{p}, δR_{B}, δR_{s} represent the spatial resolution determined by τ_{w}, B and f_{s} respectively, and τ_{r} is the detector pulse response time, which is inversely proportional to B, τ_{s} is ADC sampling interval. n is the refractive index of the core of the optical fiber. Because the application scenarios involved require relatively loose spatial resolution index, it is not discussed in detail in this paper.

4. Test verification and result analysis

A DTS-Raman system prototype and test platform are built to verify the effects of the above scheme. As shown in figure 7, a 62.5/125 μm multi-mode optical fiber is selected, of which the temperature range is −40 °C–120 °C. At room temperature, the attenuation coefficients of the optical fiber loss value are 0.509 dB km^{-1} and 0.527 dB km^{-1}, respectively. The laser pulse width emitted by the light source is 10 ns, repetition frequency is 10 kHz, and trigger mode is a self-trigger. The sampling rate of the system is 200 MHz, length of the optical fiber is 2.5 km (settable), and temperature measurement cycle is 1 s (settable).

The overall performance of the prototype is tested using the above environment to collect the backscattered Raman light and demodulate the temperature. During the test, the 2.5 km long optical fiber is placed in the room temperature environment, and some optical fibers at 0.2 km, 1.2 km and 2.4 km pass through the Asli HL-200DH temperature box, constant temperature oil bath and other instruments and are heated to 80 °C. By accumulating and averaging the collected data 10 000 times, the scattered light intensity curve is obtained in approximately 1 s, as shown in figure 8.

It can be observed from the figure that the SNR is improved obviously compared with the original echo pulse is submerged in the noise. At the same time, it can be seen that when the temperature of the environment remains constant, the light-intensity curve decreases approximately linearly with the length of the optical fiber. This is owing to the influence of temperature and laying conditions on the optical fiber loss coefficient, resulting in a slight deviation of the optical fiber loss coefficient under different conditions and the gradual weakening of the optical signal power with an increase in the optical fiber length. Then, the temperature error is getting larger and larger.

Because the sampling value of the backscattered Raman light signal contains the loss information, the optical fiber

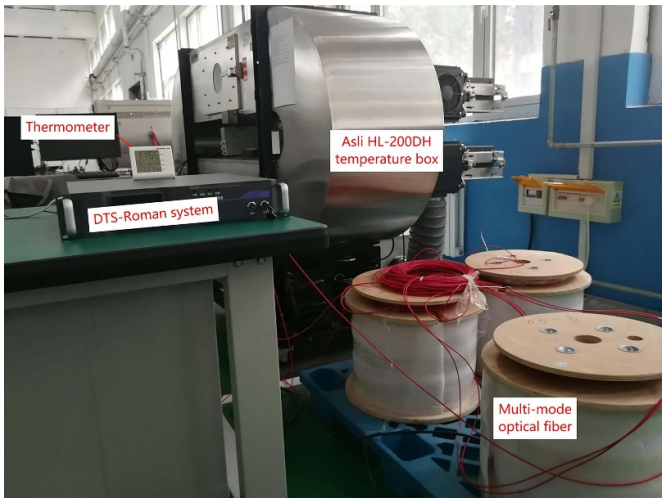

Figure 7. Prototype and test environment of DTS-Raman system.

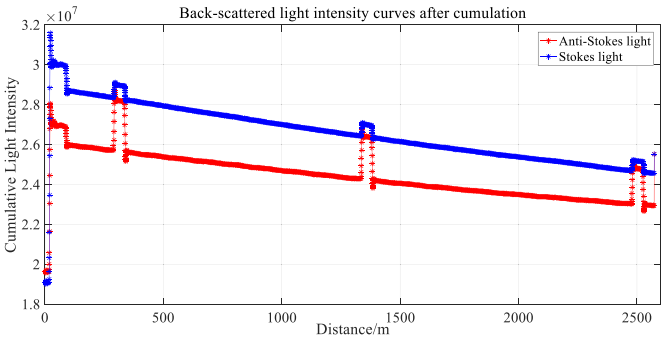

Figure 8. Schematic diagram of cumulative backscatter Raman intensity curve.

loss can be corrected according to the sampling value. Subsequently, by fitting and analyzing the actual sampling data, the temperature curve is further flattened and compensated, as shown in figure 9.

It can be seen from the figure that after optical fiber loss compensation and flattening compensation, the flatness of the temperature curve under the same temperature conditions is guaranteed. The curve reflects the temperature variation law. When the temperature of the environment in which the optical fiber is located remains constant, the temperature collected by the temperature measuring points distributed along the optical fiber layer remains constant.

In order to eliminate the inconsistent response of optical fiber temperature measuring points at different distances under different temperatures, the optical fiber is heated or cooled through the temperature box, constant temperature water tank and refrigeration constant temperature tank respectively. And the temperature values at different points after loss compensation are extracted and compared with the reference temperature set by test equipment. By multiple comparisons and data fitting, the temperature curve is leveled and compensated. The temperature response curves before and after the compensation are shown in figure 10.

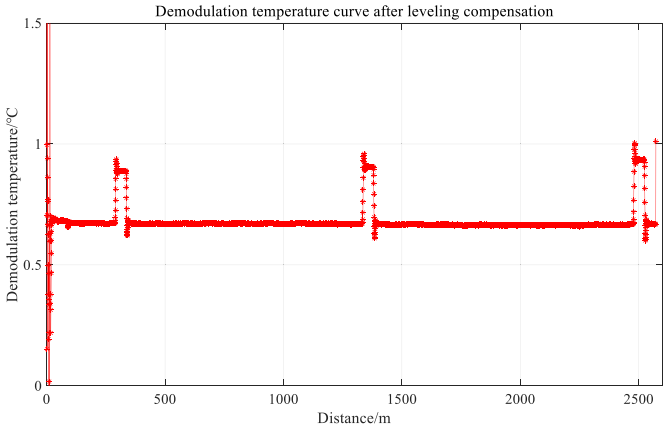

Figure 9. Schematic diagram of temperature curve after leveling compensation.

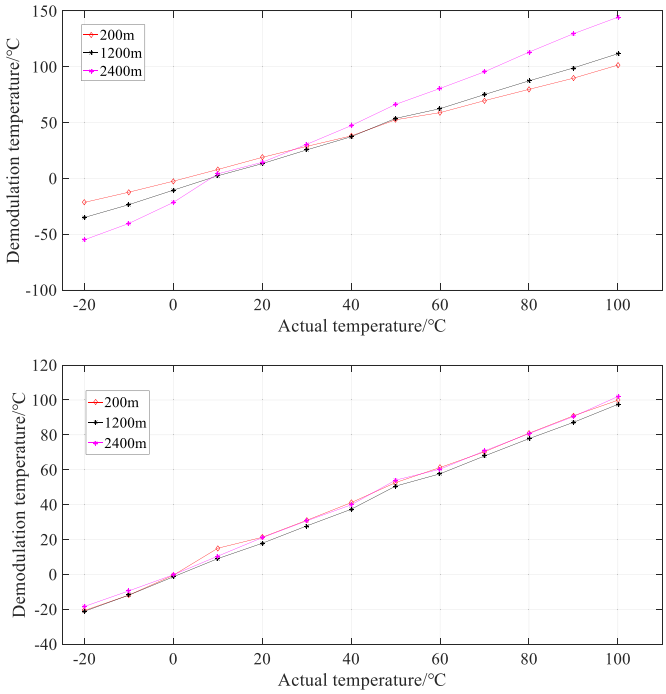

Figure 10. Comparison results before and after temperature response consistency compensation.

To eliminate the influence of system fluctuation on temperature and improve the accuracy of temperature measurement, a unified temperature linear calibration curve is obtained by fitting the temperature under different conditions. The temperature curve at room temperature after the calibration is shown in figure 11.

Through the above demodulation and calibration, the temperature measurement results of the proposed DTS-Raman system are shown in figure 12, and the specific temperature values are listed in table 3. It can be seen that the corrected temperature value fluctuates with the actual temperature at the center, and the fluctuation range is ±0.475 °C, which can meet the temperature measurement demand of ±0.5 °C.

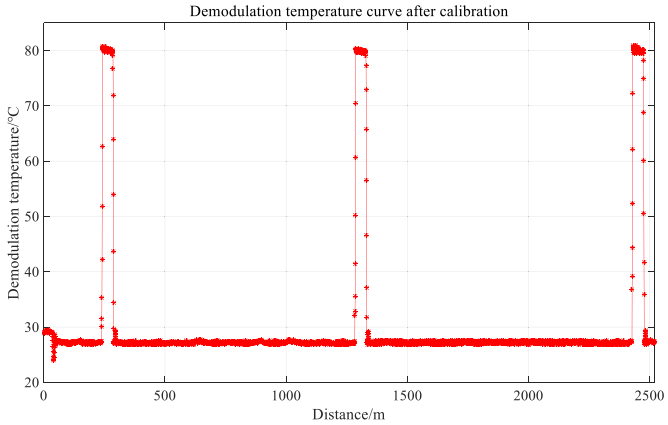

Figure 11. Temperature curve after linear calibration.

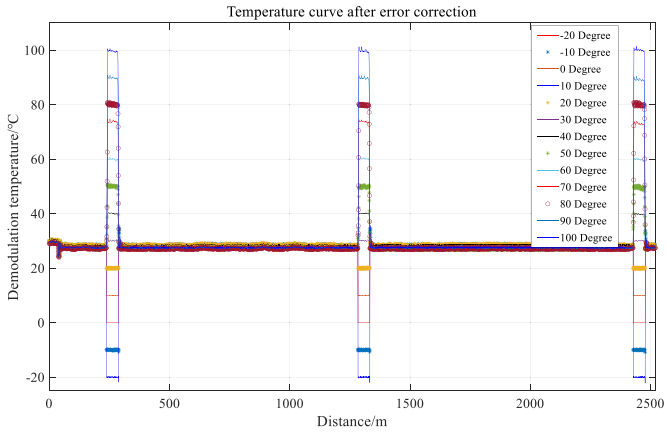

Figure 12. Temperature curve after error correction.

Table 3. Temperature measurement results after correction.

Temperature after heating (°C)	Measured temperature (°C)	Error (°C)
−20	−19.635	0.365
−10	−10.302	−0.302
0	0.431	0.431
10	9.687	−0.313
20	19.565	−0.435
30	30.433	0.433
40	39.780	−0.220
50	49.529	−0.471
60	60.439	0.439
70	69.547	−0.453
80	80.393	0.393
90	90.468	0.468
100	100.475	0.475

5. Conclusion

Based on the analysis of the principle of DTS-Raman, from the perspective of enhancing the real-time processing ability of the system and improving the resource utilization efficiency, this study discusses the noise suppression scheme and efficient implementation method in the process of temperature demodulation and proposes an implementation scheme for cumulative average denoising based on an FPGA CSRS. On this basis, a DTS prototype and test environment are built to verify the scheme. The following main conclusions are obtained:

(a) By adopting the CSRS processing architecture, the scheme realizes the recycling of storage and computing resources, which makes it possible to collect and calculate the Raman scattering light in real time on a single-chip processor, effectively improves the hardware resource utilization efficiency of the DTS-Raman system, and is conducive to miniaturization and low-cost equipment.
(b) After a series of calibrations such as cumulative average denoising, optical fiber loss compensation and temperature response consistency calibration, this scheme realizes the temperature measurement accuracy of and spatial positioning resolution of 0.5 m within the measurement range of 2.5 km. Compared with the 10 K processing speed of denoising accumulation in the traditional scheme of 2–3 s, the cumulative processing time of this scheme depends only on the repetition frequency of the laser source and the accumulated pulse number, which realizes real-time processing under controllable conditions.
(c) The prototype developed in this scheme can detect the temperature change along the optical fiber layout online, which reduces the complexity and layout cost and improves the reliability and environmental adaptability of the system. The proposed scheme has certain universality.
(d) Distributed temperature-sensing technology has the advantages of being distributed, long-distance, high-precision, and anti-interference. The measurement accuracy is not affected by the length of the optical fiber or the layout environment. Therefore, it has good application prospect for long-distance temperature monitoring and is an ideal monitoring technology.

Data availability statement

The data that support the findings of this study are available upon reasonable request from the authors.

Data access statement

All relevant data were obtained from validation tests related to the system under study and no other reference data were involved.

Conflict of interest

The authors declare that they have no known competing financial interests or personal relationships that could have influenced the work reported in this study.

Ethical statement

The study and submission was approved by all the authors.

Funding statement

The funders had no role in the study design, data collection and analysis, decision to publish, or manuscript preparation.

ORCID iD

Qigong He https://orcid.org/0000-0001-5188-5492

References

[1] Zhihui W 2020 Characteristics and research status of distributed optical fiber sensing technology *Electron. Compon. Inf. Technol.* **4** 9–10
[2] Haibin P 2019 Development and application of distributed optical fiber sensing technology *Eng. Technol. Res.* **4** 14–16
[3] Ferreira M F S and Paul M C 2021 *Optical Fiber Technology and Applications* (Bristol: IOP Publishing) pp 2053–563
[4] Xiao J and Pengfei D 2021 Research on optical fiber sensor network monitoring system for building structural health *Infrared Laser Eng.* **50** 20210263
[5] Binhua X *et al* 2019 Experiment study on pipeline bending deformation monitoring based on distributed optical fiber sensor *Chin. J. Sci. Instrum.* **40** 20–30
[6] Zhongliu Z *et al* 2020 New method to measure structure stress based on distributed optical fiber technology *Chin. J. Sci. Instrum.* **41** 45–55
[7] Haiying W *et al* 2019 Review of underground pipeline monitoring research based on distributed fiber optic sensing *J. Zhejiang Univ.* **53** 1057–70
[8] Baoqiang Y *et al* 2019 Raman distributed temperature sensor with optical dynamic difference compensation and visual localization technology for tunnel fire detection *Sensors* **19** 2320
[9] Bazzo J P, Mezzadri F, da Silva E V, Pipa D R, Martelli C and Cardozo da Silva J C 2015 Thermal imaging of hydroelectric generator stator using a DTS system *IEEE Sens. J.* **15** 6689–96
[10] Wenhua C and Zhibing C 2002 Study on distributed optical fiber temperature measuring and warning system *Infrared Laser Eng.* **02** 175–8
[11] Pervez A 1991 Multibit optical sensor networking *Proc. SPIE* 1511
[12] Yinan S *et al* 2021 Research on structural deformation estimation based on distributed optical fiber *Chin. J. Sci. Instrum.* **42** 1–9
[13] Miao Y *et al* 2021 Phase ambiguity and unwrapping of phase-sensitive optical time-domain reflectometer *Infrared Laser Eng.* **50** 229–36
[14] Genzhu W, Chunting L, Juncheng L and MA Q-Q 2021 Seven-core photonic crystal fiber temperature sensor *Opt. Precis. Eng.* **29** 951–7
[15] Tiegen L *et al* 2014 Advances in optical fiber sensing technology for aviation and aerospace application *Chin. J. Sci. Instrum.* **35** 1681–92
[16] Qin F 2016 Design and optimization of distributed optical fiber temperature measurement system based on Raman scattering *Univ. Sci. Technol. China*
[17] Bersan S, Schenato L, Rajendran A, Palmieri L, Cola S, Pasuto A and Simonini P 2017 Application of a high resolution distributed temperature sensor in a physical model reproducing subsurface water flow *Measurement* **98** 321–4
[18] Soto M A, Signorini A, Nannipieri T, Faralli S and Bolognini G 2011 High-performance Raman-based distributed fiber-optic sensing under a loop scheme using anti-Stokes light only *IEEE Photonics Technol. Lett.* **23** 534–6
[19] McDaniel A, Tinjum J M, Hart D J and Fratta D 2018 Dynamic calibration for permanent distributed temperature sensing networks *IEEE Sens. J.* **18** 2342–52
[20] Bazzo J P, Pipa D R, Martelli C, Vagner da Silva E and Cardozo da Silva J C 2016 Improving spatial resolution of Raman DTS using total variation deconvolution *IEEE Sens. J.* **16** 4425–30
[21] Jian L, Qian Z, Tao Y, Zhang M, Zhang J, Qiao L and Wang T 2020 R-DTS with heat transfer functional model for perceiving the surrounding temperature *Sensors* **20** 816–22
[22] Liping Z 2021 Design of an intelligent optical fiber grating temperature measurement system for electrical equipment *J. Phys.: Conf. Ser.* **1992** 042020
[23] Weijie W 2013 *Design and Optimization of Distributed Fiber Temperature Sensor Based on Raman Scattering* (Shandong: Shandong University)
[24] Bohao Y *et al* 2013 Design of distributed optical fiber Raman temperature sensor system based on virtual instrument *J. Optoelectron. Laser* **27** 456–60
[25] Lufei D *et al* 2014 *Radar Principles* (Beijing: Publishing House of Electronics Industry)
[26] Jinzhong X and Haipeng Z 2013 Spatial resolution improvement of distributed optical fiber Raman temperature sensor system by using amplitude modification algorithm *Key Eng. Mater.* **552** 393–7